Qing *et al. Molecular Autism* (2024) 15:43
https://doi.org/10.1186/s13229-024-00620-6

Molecular Autism

RESEARCH Open Access

Structure-function coupling in white matter uncovers the hypoconnectivity in autism spectrum disorder

Peng Qing[1], Xiaodong Zhang[1], Qi Liu[1], Linghong Huang[1], Dan Xu[1], Jiao Le[2], Keith M. Kendrick[1], Hua Lai[2*†] and Weihua Zhao[1*†]

Abstract

Background Autism Spectrum Disorder (ASD) is a neurodevelopmental disorder associated with alterations in structural and functional coupling in gray matter. However, despite the detectability and modulation of brain signals in white matter, the structure-function coupling in white matter in autism remains less explored.

Methods In this study, we investigated structural-functional coupling in white matter (WM) regions, by integrating diffusion tensor data that contain fiber orientation information from WM tracts, with functional connectivity tensor data that reflect local functional anisotropy information. Using functional and diffusion magnetic resonance images, we analyzed a cohort of 89 ASD and 63 typically developing (TD) individuals from the Autism Brain Imaging Data Exchange II (ABIDE-II). Subsequently, the associations between structural-functional coupling in WM regions and ASD severity symptoms assessed by Autism Diagnostic Observation Schedule-2 were examined via supervised machine learning in an independent test cohort of 29 ASD individuals. Furthermore, we also compared the performance of multi-model features (i.e. structural-functional coupling) with single-model features (i.e. functional or structural models alone).

Results In the discovery cohort (ABIDE-II), individuals with ASD exhibited widespread reductions in structural-functional coupling in WM regions compared to TD individuals, particularly in commissural tracts (e.g. corpus callosum), association tracts (sagittal stratum), and projection tracts (e.g. internal capsule). Notably, supervised machine learning analysis in the independent test cohort revealed a significant correlation between these alterations in structural-functional coupling and ASD severity scores. Furthermore, compared to single-model features, the integration of multi-model features (i.e., structural-functional coupling) performed best in predicting ASD severity scores.

†Hua Lai and Weihua Zhao contributed equally to this work i.e. joint corresponding authors.

*Correspondence:
Hua Lai
449535176@qq.com
Weihua Zhao
zarazhao@uestc.edu.cn

Full list of author information is available at the end of the article

© The Author(s) 2024. **Open Access** This article is licensed under a Creative Commons Attribution-NonCommercial-NoDerivatives 4.0 International License, which permits any non-commercial use, sharing, distribution and reproduction in any medium or format, as long as you give appropriate credit to the original author(s) and the source, provide a link to the Creative Commons licence, and indicate if you modified the licensed material. You do not have permission under this licence to share adapted material derived from this article or parts of it. The images or other third party material in this article are included in the article's Creative Commons licence, unless indicated otherwise in a credit line to the material. If material is not included in the article's Creative Commons licence and your intended use is not permitted by statutory regulation or exceeds the permitted use, you will need to obtain permission directly from the copyright holder. To view a copy of this licence, visit http://creativecommons.org/licenses/by-nc-nd/4.0/.

Conclusion This work provides novel evidence for atypical structural-functional coupling in ASD in white matter regions, further refining our understanding of the critical role of WM networks in the pathophysiology of ASD.

Keywords Autism spectrum disorder, Structure-function coupling, White matter tracts, Diffusion tensor, Functional connectivity tensor

Background

Autism Spectrum Disorder (ASD) is a neurodevelopmental condition associated with impairments in social and communicative abilities, along with the presence of repetitive and stereotypical behaviors and restricted interests [1]. This disorder is characterized by atypical brain connectivity patterns [2, 3] in terms of both functional and structural network alterations [4]. Previous studies utilizing diffusion tensor imaging (DTI) have revealed atypical patterns in the microstructural organization of white matter (WM) regions in individuals with ASD [5–7]. Although a significant number of studies using resting-state functional magnetic resonance imaging (rs-fMRI) have identified atypical communications within brain networks in ASD, such as the default mode network (DMN), salience network (SN) and frontoparietal networks (FPN) [8–10], these studies have primarily focused on gray matter (GM) regions, neglecting signals from WM regions.

However, similar to blood oxygen level-dependent (BOLD) signals in GM, recent studies have indicated that BOLD signals in WM are not mere "physiologically meaningless noise" but rather possess specific physiological significance [11–13]. Moreover, BOLD signals in WM exhibited varying degrees of strength and time-delay correlations within task-specific fiber pathways, which can be modulated by different tasks, highlighting their role in encoding neural activity [14–17]. In addition, resting-state data in WM has also demonstrated distinct patterns among individuals with psychiatric disorders [18, 19]. Similar to the diffusion tensor (DT) obtained in DTI, the functional connectivity tensor (FCT) can employ BOLD signals from WM to capture both the amplitude and direction of functional activation [20, 21]. Overall, the FCT approach computes the tensor representing the local spatiotemporal correlation of BOLD signals within each voxel and the tensor model quantifies functional information within WM, exhibiting the intrinsic coherence of neural activity in WM [20, 21]. Notably, this FCT feature has been used for the classification of ASD [22]. Given that BOLD signal changes in WM remain poorly understood in ASD, the utilization of the FCT approach provides a new perspective for investigating the functional connectivity disruptions within WM regions to reveal the direction of functional information transmission within WM tracts in individuals with ASD [22].

Despite increasing recognition of the importance of structural and functional coupling in ASD, the majority of studies have primarily focused on the GM [23, 24]. These studies typically employed methods that isolated the extraction of structural features from DT and functional connectivity and even predicted intrinsic functional connectivity using structural connectivity data. Due to the distinct and separate nature of functional and structural features, directly integrating them can pose limitations in revealing the precise impact of structural connections on structure-function coupling differences [4, 25]. A recent study introduced an innovative approach by combining DT, which characterizes the orientation direction of fiber tracts, with FCT, which quantifies local functional anisotropy [26]. This integrated method offers a novel approach for exploring alterations in structure-function coupling [4, 9, 27], however, this coupling on WM in ASD has rarely been explored [26].

Thus, in the current study, we aimed to: (1) explore the differences of structure-function coupling between ASD (N=89) and typically developing controls (TD) (n=63) by combining the FCT and DT data from WM tracts using the Autism Brain Imaging Data Exchange (ABIDE) II dataset; (2) investigate the relationship between clinical severity of symptoms and atypical structure-function coupling in WM using a supervised machine learning model; (3) validate the established model in an independent ASD cohort (N=29).

Methods

Participants

Discovery cohort (ABIDE-II cohort)

In this study, we utilized the ABIDE II (https://fcon_1000.projects.nitrc.org/indi/abide/) dataset [28], as a discovery dataset to investigate the alterations in structural-functional coupling in ASD. The ABIDE II dataset aggregates brain imaging data and clinical diagnostic scales collected from 19 different imaging centers worldwide and six of them were selected for the current analysis due to the availability of both DTI and rs-fMRI data. The included 6 datasets are: Barrow Neurological Institute (BNI), NYU Langone Medical Center sample 1 (NYU 1), NYU Langone Medical Center sample 2 (NYU 2), San Diego State University (SDSU), Institut Pasteur and Robert Debré Hospital (IP), and Trinity Centre for Health Sciences (TCD). Given that the DTI data from the BNI and IP sites had one missing value in both bvals (diffusion gradient strength per volume values) and bvecs (diffusion gradient directions per volume values), we excluded these two datasets. As a result, we only included the remaining

four sites, including 167 (ASD, $n=99$; TD, $n=68$) participants. Fifteen additional participants were excluded due to incomplete imaging data ($n=2$), motion artifacts (>3 mm, $n=12$), and poor signal-to-noise ratio or inadequate gray/white matter contrast ($n=1$), resulting in 89 ASD and 63 TD for the further analysis. The severity of ASD symptoms was assessed using the Autism Diagnostic Observation Schedule, Second Edition (ADOS-2) including total ADOS-2 scores, social affect (SA) and restricted and repetitive behaviors (RRB) subscale scores [29]. Only three sites collected ADOS-2 scores (NYU 1, NYU 2, SDSU, $n=76$). For the final sample size, a two-sample t-test was performed to assess differences between ASD and TD groups in demographic variables including age, Social Responsiveness Scale (SRS) total score, Full Intelligence Quotient (FIQ) standard score and Social Communication Questionnaire (SCQ). A chi-square test was used to assess the differences for gender and handedness between ASD and TD groups and all p values were corrected with False Discovery Rate (FDR).

ASD test cohort (Chengdu site)

In order to test the models trained on the discovery dataset (ABIDE II), an additional independent group of 29 children diagnosed with ASD was recruited who were scanned in Chengdu Maternal and Children's Central Hospital (CMCCH). Participants were considered eligible if they were diagnosed with ASD according to the Diagnostic Statistical Manual of Mental Disorders, Fifth Edition (DSM-V) and their diagnosis was confirmed with ADOS-2 [29], which includes social affect and restricted and repetitive behaviors subscales. Seven ASD individuals were excluded due to incomplete rs-fMRI data or DTI data, resulting in a final total of 22.

Image acquisition

The ABIDE-II data from the four included sites were as follows:

(i) NYU 1: MRI data were acquired using a 3T Siemens Allegra scanner. An anatomical T1-weighted image was acquired with a 3D magnetization prepared rapid acquisition gradient echo (MPRAGE) sequence: repetition time (TR) = 2530 ms, echo time (TE) = 3.25 ms, flip angle = 7°, FOV = 256 × 256 mm^2 and voxel size = 1.3 mm × 1.0 mm × 1.3 mm. During the rs-fMRI scan, participants were asked to relax with their eyes open, while a white cross-hair against a black background was projected on a screen, using a 2D echo planar imaging (EPI) sequence with the following parameters: TR = 2000 ms, TE = 15 ms, flip angle = 90°, FOV = 192 mm × 192 mm, matrix size = 80 × 80, voxel size = 3.0 mm × 3.0 mm × 4.0 mm, number of volumes = 180. Diffusion MRI data were acquired with 2D spinecho EPI (SE-EPI) sequence: TR = 834 ms, TE = 7.69 ms, FOV = 192 mm × 192 mm, voxel size = 3 mm × 3 mm × 3 mm 50 contiguous axial slices, 63 non-collinear gradient directions with a b value of 1000 s/mm^2 and one additional null image (b = 0 s/mm^2) as reference images.

(ii) NYU 2: MRI data were acquired using a 3T Siemens Allegra scanner. An anatomical T1-weighted image was acquired with a 3D MPRAGE sequence: TR = 2530 ms, TE = 3.25 ms, flip angle = 7°, FOV = 256 mm × 256 mm and voxel size = 1.3 mm × 1.0 mm × 1.3 mm. During the rs-fMRI scan, participants were asked to relax with their eyes open, while a white cross-hair against a black background was projected on a screen, using a 2D EPI sequence with the following parameters: TR = 2000 ms, TE = 30 ms, flip angle = 82°, FOV = 192 mm × 192 mm, matrix size = 80 × 80, voxel size = 3 mm × 3 mm × 3 mm, number of volumes = 180. Diffusion MRI data were acquired with 2D SE-EPI sequence: TR = 834 ms, TE = 7.69 ms, FOV = 192 mm × 192 mm, voxel size = 3 mm × 3 mm × 3 mm, 50 contiguous axial slices, 64 non-collinear gradient directions with a b value of 1000 s/$mm^2$and one additional null image (b = 0 s/mm^2) as reference images.

(iii) TCD: MRI data were acquired using a 3T Philips Achieva scanner. An anatomical T1-weighted image was acquired with a 3D MPRAGE sequence: TR = 8400 ms, TE = 3.90 ms, flip angle = 8°, FOV = 230 mm × 230 mm and voxel size = 0.9 mm × 0.9 mm × 0.9 mm. During the resting state scans, participants were instructed to keep their eyes directed on a cross-hair in the center of the projector, relax, and try not to fall asleep for the duration of the scan, using a 2D EPI sequence with the following parameters: TR = 2000 ms, TE = 27 ms, flip angle = 90°, FOV = 240 mm × 240 mm, matrix size = 80 × 80, voxel size = 3.0 mm × 3.0 mm × 3.2 mm, number of volumes = 210. Diffusion MRI data were acquired with 2D SE-EPI sequence: TR = 20,244 ms, TE = 79 ms, FOV = 248 mm × 248 mm, voxel size = 1.94 mm × 1.94 mm × 2 mm, 65 contiguous axial slices, 61 non-collinear gradient directions with a b value of 1500 s/mm^2 and one additional null image (b = 0 s/mm^2) as reference images.

(iv) SDSU: MRI data were acquired using a GE 3T MR750 scanner. An anatomical T1-weighted image was acquired with a 3D fast spoiled gradient echo (FSPGR) sequence: TR = 8136 ms, TE = 3.172 ms, flip angle = 8°, FOV = 256 mm × 256 mm and voxel size = 1 mm × 1 mm × 1 mm. Participants were asked to look at the red-cross for the duration

of the scan, using a 2D EPI sequence with the following parameters: TR = 2000 ms, TE = 30 ms, flip angle = 90°, FOV = 192 mm × 192 mm, matrix size = 64 × 64, voxel size = 3.438 mm× 3.438 mm × 3.4 mm, number of volumes = 180. Diffusion MRI data were acquired with 2D EPI sequence: TR = 8500 ms, TE = Minimum, FOV = 128 mm × 128 mm voxel size = 1.875 mm × 1.875 mm × 2 mm, 68 contiguous axial slices, 61 non-collinear gradient directions with a b value of 1000 s/mm and one additional null image (b = 0 s/mm^2) as reference images.

Test cohort data were collected as follows:

MRI data were acquired using a 3T Philips Ingenia scanner. All children were sedated through oral administration of chloral hydrate at a dosage of 50 mg/kg body weight, a common practice for pediatric clinical imaging. An anatomical T1-weighted image was acquired with a sagittal 3D Turbo Field Echo (TFE) sequence: TR = 8.35 ms, TE = 3.85 ms, flip angle = 8°, FOV = 512 mm × 512 mm and voxel size = 1 mm × 1 mm × 1 mm. The rs-fMRI data were acquired with eyes closed using a 2D EPI sequence with the following parameters: TR = 2000 ms, TE = 30 ms, flip angle = 77°, FOV = 128 mm × 128 mm, matrix size = 62 × 62, voxel size = 3.5 mm × 3.5 mm × 3.5 mm. A total of 220 EPI images was acquired along the AC–PC plane. Diffusion MRI data were acquired with 2D SE-EPI sequence: TR = 9298.37 ms, TE = 83.529 ms, FOV = 128 mm × 128 mm, voxel size = 2 mm × 2 mm × 2 mm, 70 contiguous axial slices, 32 non-collinear gradient directions with a b value of 1000 s/mm^2 and one additional null image (b = 0 s/mm^2) as reference images.

Image preprocessing

We preprocessed all MR data using the standardized pipeline. For rs-fMRI images, we first removed the initial 5 time points, followed by correction for slice timing and head motion effects. Subsequently, 24 motion-related parameters [30] and the mean cerebrospinal fluid (CSF) signal were regressed out to avoid elimination of signals of interest, we did not include white-matter and global brain-signal regressors. Head motion "spikes" identified by framewise displacement exceeding 0.3 mm were regressed out to minimize the potential influence of head motion on our results [27]. The data were detrended and temporally filtered with a passband frequency of 0.01–0.1 Hz [31]. Spatial smoothing within functional mask was carried out with a 6 mm at full-width at half-maximum Gaussian kernel; and co-registration to the DTI null image (b = 0 s/mm^2) along with T1-weighted images. Subjects were excluded if any of the six head motion parameters estimated during movement correction were greater than 3 mm translation or 3 degrees rotation. The rs-fMRI preprocessing was performed using SPM12 (www.fil.ion.ucl.ac.uk/spm), DPABI (http://rfmri.org/dpabi) and open MATLAB scripts (http://mind.huji.ac.il/white-matter.aspx). The preprocessing of DTI data was implemented by FSL (https://fsl.fmrib.ox.ac.uk/). First of all, we used eddy_correct to correct for eddy current distortions and motion artifacts in the diffusion-weighted images. Secondly, the bet tool was used to perform brain extraction and generate a brain mask. Finally, the dtifit tool was applied to fit the diffusion tensor model to the preprocessed data. Tissue probability maps (TPM) for GM, WM and CSF were derived by segmenting the T1-weighted images using the Computational Anatomy Toolbox (CAT12, https://neuro-jena.github.io/cat/) [32].

Definition of WM tracts

We employed the JHU ICBM-81-DTI white matter atlas (48 tracts in total) [33] to analyze white matter regions, excluding cerebellar or brainstem areas such as bilateral medial lemniscus (ML), bilateral inferior cerebellar peduncle (ICP), bilateral superior cerebellar peduncle (SCP) and bilateral inferior fronto-occipital fasciculus (IFO). The remaining 40 white matter tracts distributed within the brain region were selected to investigate the changes in structural-functional coupling in ASD [26], Abbreviations and full names of all included WM tracts are shown in Table S1. After preprocessing the DTI data, the null image was co-registered with T1-weighted images. Subsequently, the T1-weighted image was normalized to the ICBM152 T1 template in MNI space. We obtained the comprehensive transformation matrix along with its inverse matrix. Following this, we utilized the comprehensive transformation matrix to normalize each participant's co-registered multi-modal images in a similar manner. To mitigate interference from gray matter signals, templates with FA_{DT} values greater than 0.2 were included in all subsequent white matter atlases.

Construction of fractional anisotropy of functional connectivity tensor

From rs-fMRI data, we can compute the functional connectivity tensor (FCT), which characterizes the local spatial correlation patterns observed from a functional perspective of individual voxels [20]. This is analogous to the DT obtained from DTI data, which reflects the fiber orientation direction observed from a microstructural perspective [34]. First, construct a unit directional vector n_{ij}, representing the direction from voxel V_i to voxel V_j and, based on this, construct six directional vectors (x_i^2, $2x_iy_i$, $2x_iz_i$, y_i^2, $2y_iz_i$, z_i^2) for each of the 26 neighboring voxels of V_i, forming matrix M_i. Subsequently, utilizing preprocessed rs-fMRI data, Pearson linear correlation coefficients C_{ij} are calculated between the voxel V_i and the BOLD signals of its 26 neighboring voxels within a 3×3×3 neighborhood. This process forms the local

spatial correlation amplitude between V_i and its corresponding neighboring voxels. For the construction of the spatiotemporal correlation tensor T, the estimated correlations C_i projected along the vector n_i are computed, where t denotes a transpose operation:

$$C_i = n_i \cdot T \cdot n_i^t$$

After rearranging T into a column vector T_c ($T_c = [T_{xx}, T_{xy}, T_{xz}, T_{yy}, T_{yz}, T_{zz}]^t$), the relationship between C_{ij} and T_c is:

$$C_i = M_i \cdot T_c$$

a least-squares solution for T_c can be obtained as follows, -1 denotes matrix inverse:

$$T_C = (M_i^t \cdot M_i)^{-1} \cdot M_i^t \cdot C_i$$

Therefore, we can calculate the functional fractional anisotropy (FA_{FCT}) for each voxel in a manner similar to FA_{DT}. Specifically, we perform eigen-decomposition on the 3×3 tensor FCT for each voxel V_i:

$$FCT = \begin{bmatrix} T_{xx} & T_{xy} & T_{xz} \\ T_{xy} & T_{yy} & T_{yz} \\ T_{xz} & T_{yz} & T_{zz} \end{bmatrix}$$

obtaining its eigenvalues $\lambda_{i,1}$, $\lambda_{i,2}$, $\lambda_{i,3}$ and their corresponding eigenvectors, which represent the dominant directions of temporal correlation. We use FA_{FCT} values to denote the local anisotropy of spatiotemporal correlation in functional domains [22], where $\overline{\lambda} = (\lambda_{i,1} + \lambda_{i,2} + \lambda_{i,3})/3$:

$$FA_{FCT_i} = \sqrt{\frac{3}{2}} \frac{\sqrt{(\lambda_{i,1} - \overline{\lambda})^2 + (\lambda_{i,2} - \overline{\lambda})^2 + (\lambda_{i,3} - \overline{\lambda})^2}}{\sqrt{\lambda_{i,1}^2 + \lambda_{i,2}^2 + \lambda_{i,3}^2}}$$

Evaluation and validation of structure-function coupling using FCT-DT consistency

We first calculated the consistency between FCT and DT to assess structure-function coupling [26] by modifying the equation for calculating tensor differences from [35]. The FCT-DT consistency, denoted as C (T_{FCT}, T_{DT}), for each voxel is defined as:

$$C(T_{FCT}, T_{DT}) = \frac{1}{\sqrt{trace\left[(T_{FCT} - T_{DT})^2\right]}} FA_{FCT} \cdot FA_{DT}$$

T_{FCT} and T_{DT} represent the functional connectivity tensor and diffusion tensor, respectively, in a specific voxel. In general, a higher value of C indicates a greater consistency between FCT and DT. FA_{FCT} and FA_{DT} are the separate FA values of the functional connectivity tensor and diffusion tensor. However, the scales of these two tensors are not uniform. We normalize each tensor individually by utilizing the sum of all its elements, thereby ensuring that the scales across all tensors are maintained at a consistent level (Fig. 1A).

To validate that FCT-DT consistency is not randomly distributed in WM and GM regions, we compared them using the data from the TD group (N=63) of the ABIDE-II cohort. For FCT-DT consistency in WM, we calculated the mean values and overall mean of the FCT-DT consistency for each participant on the 40 white matter tracts in the JHU ICBM-81-DTI WM atlas. Individual GM masks were applied by thresholding GM TPMs at 0.8 to prevent signal contamination between WM and adjacent GM [36] and mean FCT-DT consistency within the masks compared. Initially, we compared the overall mean FCT-DT consistency for WM and GM separately. Then, we compared the mean FCT-DT consistency of each WM tract with the overall mean FCT-DT consistency in GM. Finally, to validate the internal consistency of FCT-DT in the WM region, we randomly divided the mean FCT-DT consistency of all WM tracts for each TD participant into two groups, compared the two groups 5000 times, and assessed the results. To investigate whether there were differences in FCT-DT, consistency between WM and GM, paired t-tests were conducted for the average values and individual tract value between WM and GM with FDR correction $p<0.05$. Additionally, DT, FCT and FCT-DT consistency on 40 WM tracts was compared between ASD and TD groups in WM tracts separately using two-sample t-tests with FDR correction $p<0.05$ incorporating gender, age, FIQ, handedness, and mean framewise displacement as covariates. Cohen's d values were reported as effect size.

Comparison of the predictive performance of three features with severity of ASD symptoms

Support vector regression (SVR) was conducted to investigate whether FCT (or DT, or FCT-DT) can predict ASD severity symptom using ADOS-2 subscales (RRB and SA) separately. This model is implemented using the Python scikit-learn software package (https://scikit-learn.org/stable/about.html). The SVR model (C=1) to predict the symptom severity was first conducted on the data from ABIDE II (N=76 ASD, $data_{discovery}$) using a 5-fold cross-validation (CV) approach with grid search for the model tuning controlling the regularization parameter to be relatively small to simplify the model [37–39] and the significant differences in terms of FCT, DT or FCT-DT between ASD and TD were defined as the features, respectively. This approach allowed us to train and

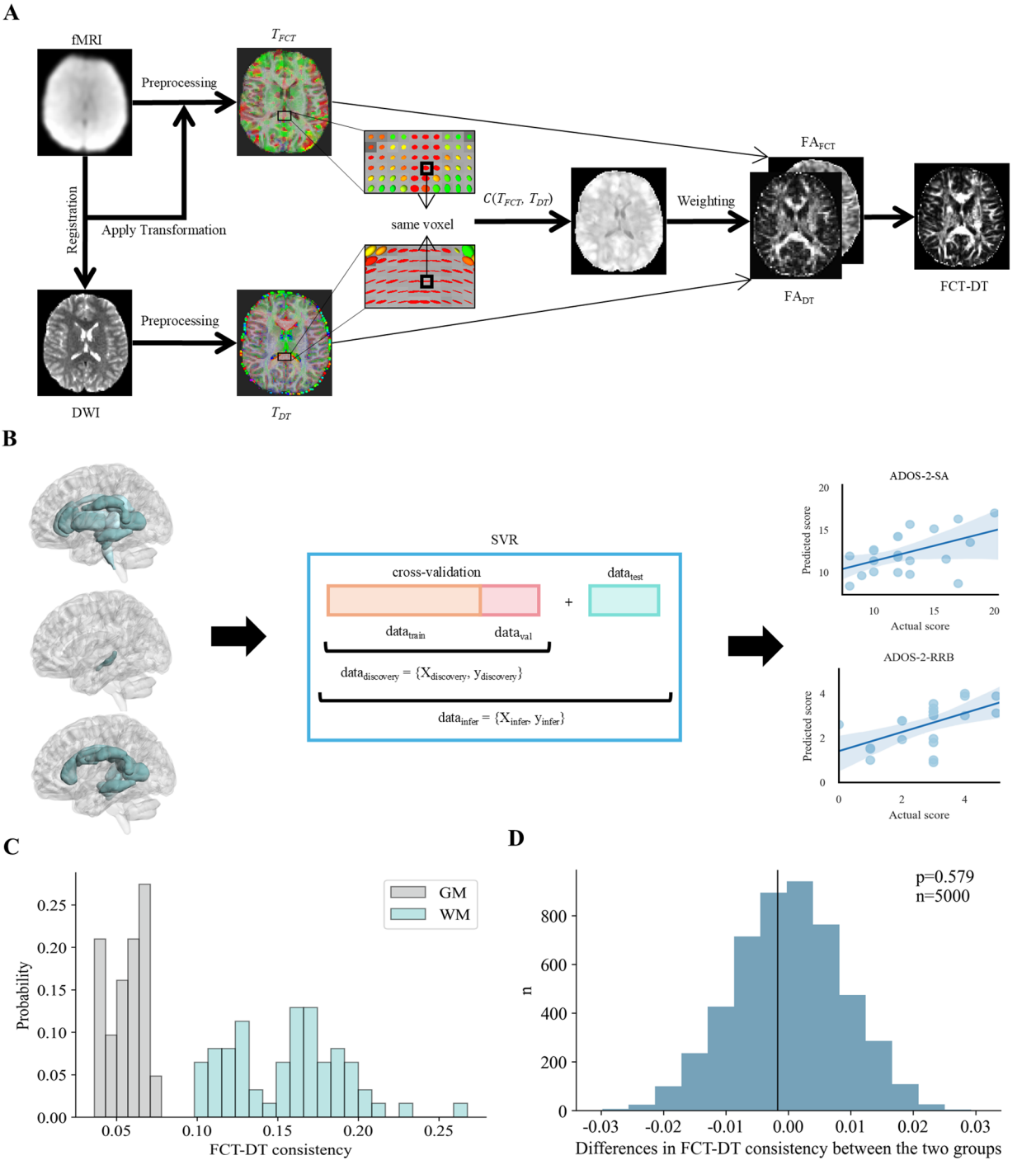

Fig. 1 Method pipeline and validation the reliability of FCT-DT consistency. **(A)** Standardized process for FCT-DT consistency. **(B)** Schematic diagram of SVR model. We trained ML models on the $data_{discovery}$ using a Five-fold cross-validation, the generalization test is performed on $data_{infer}$ by using the $data_{test}$ as the test data. **(C)** The distribution of FCT-DT consistency within the GM and WM. **(D)** The internal consistency of FCT-DT consistency was examined by comparing group differences within the TD group. Abbreviations: DWI, diffusion weighted imaging; FA, functional anisotropy; SVR, support vector regression; ADOS-2, autism diagnostic observation schedule 2nd edition; SA, social affect; RRB, restricted and repetitive behaviors. GM, gray matter; WM, white matter

validate the entire dataset separately, providing a comprehensive assessment of the model's performance and enabling us to select the optimal model hyperparameters, thus avoiding overfitting on a single dataset. Subsequently, the developed SVR models were performed 5000 times, with different random seeds to reassign the training and validation dataset each time, thereby avoiding subject selection bias [40]. The final SVR models were trained on all ASD individuals from ABIDE-II for further generalization on the Chengdu site (N=22 ASD, Fig. 1B). Finally, the performance of these trained models using different features (FA_{FCT}, FA_{DT}, and FCT-DT) were compared. Permutation tests (repeated 5000 times) were employed to examine the statistical significance of the model's regression coefficients [41] with mean absolute error (MAE) measuring the average of the absolute error between the predicted and true values. Furthermore, considering the multi-site and multi-modal nature of the dataset utilized in our study, we employed Combat harmonization [42] (https://github.com/Jfortin1/ComBatHarmonization) as a correction method to eliminate site differences in these three key features (FA_{DT}, FA_{FCT}, FCT-DT). Subsequently, we constructed a covariate matrix, including sex, age, FIQ, handedness, mean framewise displacement. To ensure data consistency across batches, we standardized the data and applied a consistent five-fold CV method for training, validation and test datasets.

Additionally, to test the model's robustness, leave-one-site-out cross generalization (CG) was conducted across the three different sites in the discovery cohort and findings validated in the test cohort ($data_{test}$) we collected (N=22 ASD). In other words, subjects from any two of the 3 recruitment sites of ABIDE-II were used as the training dataset and validated the models in the Chengdu site. Permutation tests (repeated 5000 times) were also conducted to examine the statistical significance of the model.

Table 1 Clinical and demographic characteristics (mean ± SD)

Characteristic	ASD	TD	Statistic value	*p* value
Age (years)	11.07 ± 5.29	12.85 ± 4.12	-1.23	0.232[a]
Sex	79 boys/10 girls	60 boys/3 girls	1.98	0.161[b]
Handedness	68 R/7 L/14 M	57 R/2 L/4 M	5.00	0.082[b]
FIQ	104.38 ± 17.02	113.11 ± 14.17	-3.33	0.001[a]
SRS	78.12 ± 13.06	43.25 ± 6.21	19.34	< 0.001[a]
SCQ	16.44 ± 7.41	2.57 ± 2.03	14.21	< 0.001[a]
ADOS-2 SA	3.28 ± 1.93	-	-	-
ADOS-2 RRB	9.91 ± 3.75	-	-	-
ADOS-2 TOTAL	13.18 ± 4.64	-	-	-

[a]Two-sample t test

[b]Chi-squared test

All p values were original without any correction. Abbreviations: SD, standard deviation; R, right handed; L, left handed; M, mixed handed; FIQ, full intelligence quotient standard score; SRS, social responsiveness scale total score; SCQ, social communication questionnaire; ADOS-2, autism diagnostic observation schedule 2nd ed; RRB, restricted and repetitive behaviors; SA, social affect

Results

Demographic and clinical characteristics

The demographic and clinical characteristics between 89 ASD (79 boys; age: 11.07±5.29 years) and 63 TD (60 boys; age: 12.85±4.12 years) individuals with rs-fMRI and DTI data from ABIDE II dataset were compared (**see** Table 1). There were no significant differences between the two groups in terms of age (p=0.23), sex (p=0.19), and handedness (p=0.12). The FIQ (p=0.002), SRS (p<0.001), and SCQ (p<0.001) scores of the ASD group were significantly lower than those of the TD group. In the test cohort, we analyzed a sample of 22 ASD children (18 boys, age: 6.64±1.30) with rs-fMRI and DTI data, as well as ADOS-2 assessment (total score: 15.23±3.78; SA: 2.77±1.27; RRB: 12.45±3.49). There was no significant difference in ADOS-2 scores between the ABIDE-II cohort and our own cohort (all ps>0.06), although there was for age (t=3.89, p<0.001).

Evaluation and validation of FCT-DT consistency

To assess the reliability of the FCT-DT consistency in WM, a validation analysis was conducted by comparing the consistency of the coupling coefficient between the average values of WM and GM in the TD group. Compared to GM, the averaged FCT-DT consistency in the WM tracts exhibited significantly stronger structure-function coupling (t=16.66, p<0.001; Fig. 1C), and the mean value in each individual WM tract also showed significantly stronger structure-function coupling compared to GM (Fig. S1 and Table S2). Additionally, the internal consistency of the FCT-DT consistency was assessed by comparing inter-group differences within the TD group and there was no significant difference in WM (p>0.57; Fig. 1D).

Comparison of group differences in WM tracts through FCT-DT consistency

The FCT-DT consistency showed significant reductions in the ASD group compared to the TD group in a number of WM tracts, including the corpus callosum (GCC: t = -2.67, FDR_corrected p=0.043, Cohen's d=0.44; BCC: t = -2.78, FDR_corrected p=0.043, Cohen's d=0.45; SCC: t = -2.89, FDR_corrected p=0.043, Cohen's d=0.47), right cerebral peduncle (t = -2.62, FDR_corrected p=0.043, Cohen's d=0.43), left retrolenticular part of internal capsule (t = -2.44, FDR_corrected p=0.049, Cohen's d=0.40), left posterior thalamic radiation (t = -2.64, FDR_corrected p=0.043, Cohen's d=0.43), left sagittal stratum (t = -2.60, FDR_corrected p=0.043, Cohen's d=0.43), cingulum (bilateral cingulum (cingulate gyrus), left: t =

-2.44, FDR_corrected p=0.049, Cohen's d=0.40; right: t = -2.38, FDR_corrected p=0.049, Cohen's d=0.39; right cingulum (hippocampus), t = -2.57, FDR_corrected p=0.049, Cohen's d=0.42), bilateral fornix (cres) stria terminalis (t = -2.64, left: FDR_corrected p=0.049, Cohen's d=0.43; right: t = -2.74, FDR_corrected p=0.043, Cohen's d=0.45), left superior longitudinal fasciculus (t = -3.01, FDR_corrected p=0.043, Cohen's d=0.49) and left superior fronto-occipital fasciculus (t = -2.57, FDR_corrected p=0.043, Cohen's d=0.42) (Fig. 2 and Fig. S2). All WM tracts with uncorrected p values are shown in Table S3.

Predictive model of FCT-DT for assessing severity of ASD symptoms

We firstly compared performance of three predictive models based on FA_{DT}, FA_{FCT} (Table S4 and Table S5) and FCT-DT features respectively for assessing severity of ASD symptoms using the ADOS-2 subscales (SA and RRB, Fig. 3A and Fig. S3). Five-fold CV analyses showed that the differences of FA_{DT} between ASD and TD significantly predicted the SA (mean±SD r=0.247±0.0195; MAE=3.055±0.033; p=0.021) and RRB (mean±SD r=0.287±0.0282; MAE=1.501±0.032; p=0.011) scores. The group differences for FA_{FCT} were not predictive for any of the subscale scores (all ps>0.087, Fig. S4). Notably, the FCT-DT consistency can significantly predict both the SA (mean±SD r=0.323±0.041; MAE=2.774±0.047; p=0.007) and the RRB scores (mean±SD r=0.353±0.031; MAE=1.483±0.011; p=0.003) with greater predictive performance (FCT-DT vs. FA_{DT}, SA: t=153.043, FDR_corrected p<0.001; RRB: t=175.947, FDR_corrected p<0.001, Fig. 3B) using t-tests. Additionally, the results with ComBat harmonization suggested that FCT-DT consistency could significantly predict SA (mean±SD r=0.27±0.42; MAE=2.93±0.06; p=0.023) and RRB scores (mean±SD r=0.30±0.13; MAE=1.55±0.07; p=0.006) but not that of the other two features (FA_{DT}, FA_{FCT}, ps>0.067, Fig. S6). Furthermore, the trained FA_{DT} model based on the ABIDE-II cohort could significantly predict the SA (r=0.439; MAE=2.373; p=0.041) and the RRB scores (r=0.498; MAE=1.149; p=0.018) in our independent cohort, however, the FA_{FCT} model could not (all ps>0.136, Fig. S4). The trained FCT-DT consistency model is predictive of both the SA (r=0.517; MAE=2.295; p=0.014) and the RRB scores (r=0.557; MAE=0.780; p=0.007, Fig. 3C). Even after ComBat harmonization, the FCT-DT consistency model maintains its predictive power, allowing for the prediction of both the SA (r=0.457; MAE=2.347; p=0.033) and the RRB scores (r=0.504; MAE=0.925; p=0.017).

Additionally, leave-one-site-out CG analyses indicated that the FA_{DT} significantly predicted RRB scores (mean±SD r=0.36±0.12; MAE=1.02±0.07; p=0.031), but not SA scores (mean±SD r=0.32±0.08; MAE=3.03±0.12; p=0.092). The FA_{FCT} did not show any predictive performance on the severity of ASD symptom sub-scores (all ps>0.183, Fig. S5). More importantly, the FCT-DT consistency significantly predicted the SA (mean±SD r=0.45±0.06; MAE=2.55±0.06; p=0.011) and the RRB scores (mean±SD r=0.44±0.11; MAE=0.96±0.09; p=0.026, Fig. 3D). Overall, these results indicated that the integration of multi-modal based FCT-DT consistency significantly predicted the autism severity scores better than the two single models.

Discussion

In the current study, we examined alterations in structural-functional coupling, which captured spatial and temporal consistency of functional signals with diffusion tensor orientations in WM networks from functional and diffusion magnetic resonance images. Our findings indicate that individuals with ASD exhibit widespread reductions in structural-functional coupling in WM regions in commissural tracts (e.g. corpus callosum), association tracts (sagittal stratum), and projection tracts (e.g. internal capsule) compared to TD individuals. Notably, among the single and multi-modal models, these alterations in the integrated structural-functional coupling demonstrate significant predictive potential for ASD severity symptom. The current results support the dysconnectivity hypothesis of ASD from structural and functional integration, and highlight the pivotal role of WM networks in the pathophysiology of ASD.

FCT analogous to the DT in WM tracts

The FCT can describe the functional structure consistent with the fiber tracts visualized by independent structural imaging (DT) and can be detected during the resting state, as well as enhanced by performance of related functional tasks [20, 43]. Therefore, we hypothesize that FCT and DT not only exhibit similarity in representing WM structure but also complement each other in their respective strengths (DT better shows structural directionality, while FCT better reflects functional correlation). Mathematically, both are tensor structures consisting of 3×3 symmetric, positive-definite matrices, containing three eigenvalues ($\lambda_{i,1}$, $\lambda_{i,2}$, $\lambda_{i,3}$) and their corresponding eigenvectors. In DT, the three eigenvectors reflect the three diffusion directions of water molecules, and the eigenvalues indicate the degree of diffusion in each direction. In FCT, the three eigenvectors reflect the temporal correlation preferences of BOLD signals between each voxel and adjacent voxels, and the eigenvalues indicate the degree of correlation in each direction [22]. Therefore, we believe that both can be analyzed using the same approach from mathematical and neurobiological perspectives. Thus, the calculation of FCT can be thoroughly analogous to that of DT [26].

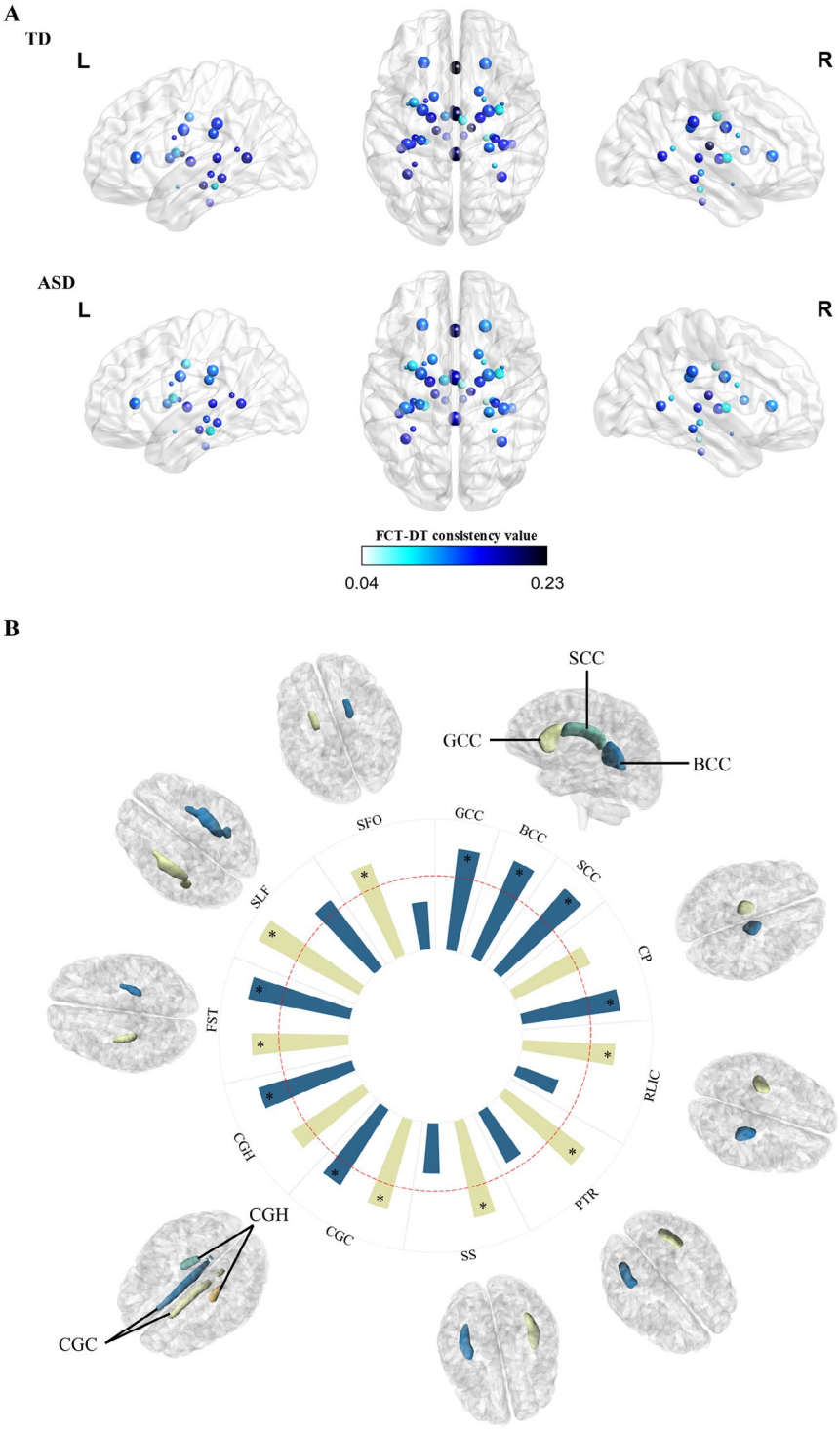

Fig. 2 The group differences in FCT-DT consistency in the WM tracts. **(A)** The FCT-DT consistency of each WM tract in the ASD group and TD group. The size of a node is directly proportional to the volume of the corresponding white matter tract, implying that a larger node corresponds to a greater volume of the white matter tract. Meanwhile, the color of a node is positively correlated with the consistency of FCT-DT, where darker colors indicate a higher degree of consistency. **(B)** Between-group differences in FCT-DT consistency. The inner circular bars represent *t*-values of the corresponding WM tract. The red dashed circle represents $p = 0.05$ uncorrected, * $p < 0.05$ after FDR correction. Abbreviations: GCC, genu of corpus callosum; BCC, body of corpus callosum; SCC, splenium of corpus callosum; CP, cerebral peduncle; RLIC, retrolenticular part of internal capsule; PTR, posterior thalamic radiation; SS, Sagittal stratum; CG, cingulum; FST, fornix (cres) stria terminalis; SLF, superior longitudinal fasciculus; SFO, superior fronto-occipital fasciculus

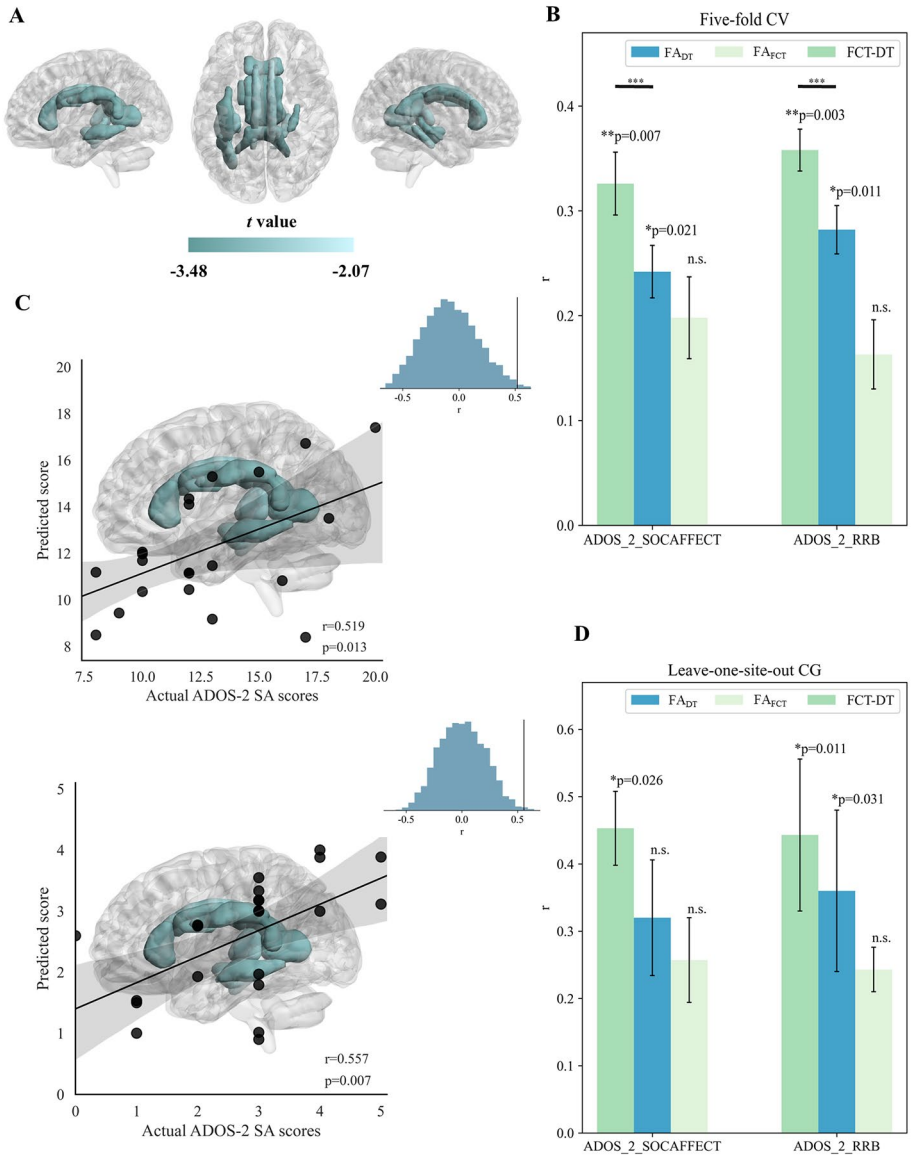

Fig. 3 Predictive performance of single-modal and multi-modal models with autism symptoms. **(A)** Significant WM tracts with substantial differences in the FCT-DT consistency. The color of WM tracts corresponds to the *t* value. **(B)** Comparisons between the predictive models using Five-fold CV respectively, where the error bars indicate SD. *** indicates $p < 0.001$ after FDR correction for the two-sample t-test between the two groups. Statistical significance is obtained from 5000 permutation tests and shown with ** $p < 0.01$, * $p < 0.05$, and 'n.s.', no significant. **(C)** The scatter plot shows the correlation between predicted values and true severity of autism symptoms in the test set. The model used was trained on FCT-DT-consistent feature, severity was assessed using ADOS-2 SA and RRB subscale scores. The background shading indicates the selected feature regions. The histogram represents a surrogate distribution comprising r values for the same feature data with shuffled labels, vertical black line denotes r value of ground-truth script type. **(D)** To thoroughly assess the inter-site stability of a prediction model, the leave-one-site-out CG approach is employed independently for each site, where the error bars indicate SD. Statistical significance is obtained from 5000 permutation tests and shown with ** $p < 0.01$, * $p < 0.05$, and 'n.s.', no significant. Abbreviations: CV, cross-validation; CG, cross generalization; SD, standard deviation; ADOS-2, autism diagnostic observation schedule 2nd ed; SOCAFFECT, social affect; RRB, restricted and repetitive behaviors

ASD individuals exhibit reductions in structural-functional coupling in the WM tracts

Although ASD studies have primarily focused on GM regions [44], a growing number of studies have suggested that ASD individuals also exhibit structural alterations in white matter [3, 45, 46]. The WM signals are essential for interconnecting and facilitating information transmission between various brain regions [13]. Additionally, white-matter functional networks are associated with behavioral deficits in ASD [46]. Thus, analyzing white matter

may offer a unique opportunity to track atypical processes in ASD, considering its crucial function in facilitating neuronal migration [47].

Furthermore, multi-modal connectivity networks between the brain's anatomical structural connectome and its physiological functional connectome have been determined in healthy and clinical populations [4, 22, 23, 25, 26]. In the current study, 9 out of 40 WM tracts exhibited significantly lower structure-function coupling than those in the TD group, indicating dysconnectivity in ASD with atypical connectivity between regions affecting the functions of neural circuits.

Specifically, a decrease in structure-function coupling was observed in the corpus callosum. The corpus callosum can be categorized as a commissural pathway, serving as the primary fiber tract that connects the two cerebral hemispheres. It facilitates integrated interhemispheric communication between homotopic (functionally similar) and heterotopic (functionally distinct) cortical regions, enabling the exchange of information and coordination of functions between the two brain hemispheres [48]. Furthermore, previous studies have revealed atypical structure and diffusion characteristics in ASD, which have been linked to repetitive behaviors and sensory responsiveness in infants at high risk [5, 49–51]. A meta-analysis has revealed a moderate reduction in the total corpus callosum area in ASD, aligning with studies that implicate the corpus callosum in emotional and social functioning as well as higher cognitive processes such as decoding non-literal meaning, affective prosody, and humor comprehension [52]. In a study on twins where at least one twin was diagnosed with ASD genetic factors also appeared to exert the greatest impact on brain-behavior relationships between white matter integrity, particularly of commissural fibers (i.e. corpus callosum) and general cognitive abilities [53]. Disruptions in corpus callosum mediated inter-hemispheric communication may underlie numerous sensory, cognitive, and behavioral symptoms observed in children with ASD [54].

While previous studies have yielded inconsistent findings regarding fractional anisotropy in the cerebral peduncle and internal capsule between ASD and TD individuals [55–57], our current study has revealed widespread reductions in structure-function coupling in these WM tracts relative to the TD group. Specifically, we observed reductions in projection pathways, particularly the vertically projecting tracts that connect cortical regions to subcortical nuclei or brainstem regions. These affected tracts include the cerebral peduncle, the retrolenticular segment of the internal capsule, and the posterior thalamic radiation [58]. Such reductions in WM tracts may indicate a loss of integrity in motor and somatosensory function or tactile perception [57].

Additionally, the association pathway [58] comprises tracts that are oriented along the anterior-posterior axis, including the bilateral cingulum, sagittal stratum, bilateral fornix (cres) stria terminalis, superior longitudinal fasciculus and superior fronto-occipital fasciculus decreased in ASD. The cingulum, a crucial fiber system connecting the cingulate and surrounding medial cortex to medial temporal lobe internally, plays a significant role in social and emotional functions linked to the core symptomatology of ASD [59]. Reduced fractional anisotropy in the cingulum is frequently observed in ASD. Additionally, lesions in the longitudinal fasciculus and fronto-occipital fasciculus have been associated with impaired processing of affective facial expressions [60] as well as language production [61]. The sagittal stratum, a fiber complex encompassing the longitudinal fasciculus, fronto-occipital fasciculus and other subcortical structures, has been functionally associated with visually guided behaviors, such as face-based mentalizing [62]. Individuals with ASD who demonstrate slower sagittal stratum development tend to show increased severity of symptoms over time [63], , suggesting a potential correlation between sagittal stratum and ASD progression. Overall, the association pathway appears to be linked to affective emotional processing, and the observed reductions in this pathway may suggest a potential marker for ASD.

Furthermore, the commissural pathway traverses the deep white matter, intersecting both the association and projection pathways. In essence, reduced diffusion anisotropy in white matter regions, such as the corpus callosum, may signify disorganization or abnormal development of projection, commissural and association fibers. This, in turn, could be associated with impairments in functional domains that rely on efficient interhemispheric information transfer [64]. This pathway facilitates communication between symmetrical regions of the brain hemispheres [48, 58]. Thus, reductions in these pathways are implicated in the motor, emotional and inter-hemispheric communication difficulties observed in ASD.

The associations between ASD severity and the changes in structural-functional coupling

In comparison to single modal imaging techniques (such as DT or FCT), multi-modal features have the greater potential to serve as a more stable neural marker for predicting ASD severity, both in the discovery cohort and our test cohort. Consistent with previous studies demonstrating fractional anisotropy (FA_{DT}) as a sensitive single modal feature in certain WM tracts and clinical loads [5, 65], our current study also found that fractional anisotropy in commissural tracts (e.g. corpus callosum), association tracts (sagittal stratum), projection tracts (e.g.

internal capsule, see supplementary table) was predictive of ADOS-2 scores for social affect, as well as restricted and repetitive behaviors, in both the ABIDE-II cohort and our independent cohort using five-fold cross validation. However, when applying the leave-one-site-out cross generalization approach, it was observed that this feature was predictive only for restricted and repetitive behaviors, and not for social affect, suggesting that fractional anisotropy may not be sufficiently stable and could be influenced by factors such as age [63]. On the other hand, the developed structure-function coupling (i.e. FCT-DT consistency in WM) showed robust predictive performance in both the ABIDE-II cohort and our independent cohort, regardless of the validation or generalization approach used. Remarkably, the predictive performance of this coupling with clinical severity surpassed that of fractional anisotropy alone. The robust role of structure-function coupling in the WM tracts has been emphasized in the pathophysiology of ASD by the current study, reflecting the integrity of neural signals linked to cognition and disorder through the fundamental characteristic of the association between structure and function [66–69].

Potential limitations

This study has several potential limitations that should be acknowledged. Firstly, due to the absence of ADOS-2 assessments, we were only able to include a relatively small sample size of 76 individuals with ASD in the training dataset. This may have somewhat reduced the statistical power of our results, even though we conducted a leave-one-site-out cross generalization approach and verified the reliability of the structure-function coupling in predicting severity. Secondly, there was a significant difference in age between the ABIDE-II cohort and our own test cohort. Acquisition of DTI and resting-state data from autistic individuals can be challenging. Although the structure-function coupling, when harmonized using Combat, serves as a reliable and robust neural marker for predicting severity across different ages and scanners, this age discrepancy between cohorts may have introduced additional variability. Additionally, composite indices of brain structure and function were not associated with age among individuals with ASD [11], thus suggesting they were independent of age in ASD. Thirdly, the evaluation of structure-function coupling using FCT-DT consistency was less reliable in regions with crossing fibers. This limitation stems from the inherent constraint of the tensor model, which can only depict a single primary fiber direction per voxel, coupled with the heightened vulnerability of crossing fibers due to issues related to overlapping fiber tracts, as compared to non-crossing fibers [48, 58, 70]. Despite the fact that both FCT and DT exhibit similarities in characterizing WM structure, they also exhibit complementary strengths [20, 26]. This suggests that both tensors may only capture a fraction of the WM connections, thereby impacting the reliability of using FCT-DT consistency to infer structure-function coupling in regions with crossing fibers.

Finally, the children in the test cohort were sedated through oral administration of chloral hydrate, which differs from the children from ABIDE-II cohort. This potential difference in sedation methods may impact their brains [71] and subsequently influence our results. However, it's important to note that other studies have also successfully used chloral hydrate for acquiring MRI data in children with ASD, and it is generally considered safe with minimal side effects for this purpose [72–74]. However, our study found that both trained FCT-DT consistency models, based on the ABIDE-II cohort with and without ComBat harmonization [42], consistently predict symptom severity in our independent cohort. This suggests that the sedation method used did not have a notable impact on the structural-functional coupling results observed in both cohorts.

Conclusion

In summary, our observed widespread decreases in the structure-function coupling within WM tracts among individuals with ASD provides support for the initial dysconnectivity hypothesis of ASD from a WM functional perspective. These reductions may be attributed to aberrant neural signal propagation along WM tracts. Moreover, the associations between clinical symptoms and structure-function coupling in the WM tracts suggested that atypical structure-function coupling could be a potential neuropathological mechanism underlying ASD. Collectively, these findings possess extensive significance for understanding atypical development associated with neuropsychiatric disorders, particularly ASD.

Supplementary Information

The online version contains supplementary material available at https://doi.org/10.1186/s13229-024-00620-6.

Supplementary Material 1

Acknowledgements

We would like to thank the contributors and organizers of the Autism Brain Imaging Data Exchange II (http://fcon_1000.projects.nitrc.org/indi/abide/).

Author contributions

P.Q. and W.Z. designed research; P.Q., L.H. and W.Z. collected the data; P.Q., X.Z. and W.Z performed research; P.Q. and Q.L. drafted the manuscript. D.X. and J.L. provided guidance and advice; H.L., K.M.K. and W.Z. provided feedback and revised the manuscript.

Funding

This work was supported by the Natural Science Foundation of Sichuan Province [grant number 2022NSFSC1375 - WHZ], Humanity and Social Science Foundation of Ministry of Education of China [grant number 24YJC190046 - WHZ], National Natural Science Foundation of China (NSFC) [grant number

82301732- JL], Sichuan Province Key Research and Development Project [grant number 2023YFWZ0003 - KMK].

Data availability

The datasets supporting the conclusions of this article are available in the Autism Brain Imaging Data Exchange II (http://fcon_1000.projects.nitrc.org/indi/abide/). The scripts for FCT and FCT-DT consistency are available in github (https://github.com/zhaolab205/ASD-FCT-DT-consistency).

Declarations

Ethics approval and consent to participate

The study has been approved by the local ethics committee of the University of Electronic Science and Technology of China and followed with the latest revision of the declaration of Helsinki. All written informed consent was provided by participants' parents or legal guardians.

Competing interests

The authors declare no competing interests.

Author details

[1]The Center of Psychosomatic Medicine, Sichuan Provincial Center for Mental Health, Sichuan Provincial People's Hospital, University of Electronic Science and Technology of China, Chengdu 611731, China
[2]Chengdu Women's and Children's Central Hospital, School of Medicine, University of Electronic Science and Technology of China, Chengdu 611731, China

Received: 3 June 2024 / Accepted: 11 September 2024
Published online: 04 October 2024

References

1. Lord C, Charman T, Havdahl A, Carbone P, Anagnostou E, Boyd B, et al. The Lancet Commission on the future of care and clinical research in autism. Lancet. 2022;399:271–334.
2. Müller R-A, Fishman I. Brain Connectivity and Neuroimaging of Social Networks in Autism. Trends Cogn Sci. 2018;22:1103–16.
3. Sato W, Uono S. The atypical social brain network in autism: advances in structural and functional MRI studies. Curr Opin Neurol. 2019;32:617–21.
4. Park B, Benkarim O, Weber CF, Kebets V, Fett S, Yoo S, et al. Connectome-wide structure-function coupling models implicate polysynaptic alterations in autism. NeuroImage. 2024;285:120481.
5. Aoki Y, Yoncheva YN, Chen B, Nath T, Sharp D, Lazar M, et al. Association of White Matter structure with autism spectrum disorder and Attention-Deficit/Hyperactivity disorder. JAMA Psychiatry. 2017;74:1120–8.
6. Huang X, Ming Y, Zhao W, Feng R, Zhou Y, Wu L, et al. Developmental prediction modeling based on diffusion tensor imaging uncovering age-dependent heterogeneity in early childhood autistic brain. Mol Autism. 2023;14:41.
7. Solso S, Xu R, Proudfoot J, Hagler DJ, Campbell K, Venkatraman V, et al. Diffusion Tensor Imaging provides evidence of possible Axonal Overconnectivity in Frontal lobes in Autism Spectrum Disorder toddlers. Biol Psychiatry. 2016;79:676–84.
8. Buch AM, Vértes PE, Seidlitz J, Kim SH, Grosenick L, Liston C. Molecular and network-level mechanisms explaining individual differences in autism spectrum disorder. Nat Neurosci. 2023;26:650–63.
9. Holiga Š, Hipp JF, Chatham CH, Garces P, Spooren W, D'Ardhuy XL, et al. Patients with autism spectrum disorders display reproducible functional connectivity alterations. Sci Transl Med. 2019;11:eaat9223.
10. Uddin LQ. Brain mechanisms supporting flexible cognition and behavior in adolescents with Autism Spectrum Disorder. Biol Psychiatry. 2021;89:172–83.
11. Chen B, Olson L, Rios A, Salmina M, Linke A, Fishman I. Reduced covariation between brain morphometry and local spontaneous activity in young children with ASD. Cereb Cortex. 2024;34:112–20.
12. Gawryluk JR, Mazerolle EL, D'Arcy RCN. Does functional MRI detect activation in white matter? A review of emerging evidence, issues, and future directions. Front Neurosci. 2014;8:239.
13. Schilling KG, Li M, Rheault F, Gao Y, Cai L, Zhao Y, et al. Whole-brain, gray, and white matter time-locked functional signal changes with simple tasks and model-free analysis. Proc Natl Acad Sci. 2023;120:e2219666120.
14. Huang Y, Bailey SK, Wang P, Cutting LE, Gore JC, Ding Z. Voxel-wise detection of functional networks in white matter. NeuroImage. 2018;183:544–52.
15. Mishra A, Li M, Anderson AW, Newton AT, Ding Z, Gore JC. Concomitant modulation of BOLD responses in white matter pathways and cortex. NeuroImage. 2020;216:116791.
16. Yang Y, Wang S, Liu J, Zou G, Jiang J, Jiang B, et al. Changes in white matter functional networks during wakefulness and sleep. Hum Brain Mapp. 2022;43:4383–96.
17. Zu Z, Choi S, Zhao Y, Gao Y, Li M, Schilling KG, et al. The missing third dimension-functional correlations of BOLD signals incorporating white matter. Sci Adv. 2024;10:eadi0616.
18. Ji G-J, Sun J, Hua Q, Zhang L, Zhang T, Bai T, et al. White matter dysfunction in psychiatric disorders is associated with neurotransmitter and genetic profiles. Nat Ment Health. 2023;1:655–66.
19. Jiang Y, Luo C, Li X, Li Y, Yang H, Li J, et al. White-Matter functional networks changes in patients with schizophrenia. NeuroImage. 2019;190:172–81.
20. Ding Z, Xu R, Bailey SK, Wu T-L, Morgan VL, Cutting LE, et al. Visualizing functional pathways in the human brain using correlation tensors and magnetic resonance imaging. Magn Reson Imaging. 2016;34:8–17.
21. Li M, Newton AT, Anderson AW, Ding Z, Gore JC. Characterization of the hemodynamic response function in white matter tracts for event-related fMRI. Nat Commun. 2019;10:1140.
22. Wang J, Zhang L, Wang Q, Chen L, Shi J, Chen X, et al. Multi-class ASD classification based on functional connectivity and functional correlation Tensor via Multi-source Domain Adaptation and Multi-view sparse representation. IEEE Trans Med Imaging. 2020;39:3137–47.
23. Benkarim O, Paquola C, Park B, Hong S-J, Royer J, De Vos R, et al. Connectivity alterations in autism reflect functional idiosyncrasy. Commun Biol. 2021;4:1078.
24. Hong S-J, Mottron L, Park B, Benkarim O, Valk SL, Paquola C, et al. A convergent structure–function substrate of cognitive imbalances in autism. Cereb Cortex. 2023;33:1566–80.
25. He C, Chen H, Uddin LQ, Erramuzpe A, Bonifazi P, Guo X, et al. Structure–function Connectomics reveals aberrant developmental trajectory occurring at Preadolescence in the autistic brain. Cereb Cortex. 2020;30:5028–37.
26. Zhao J, Huang C-C, Zhang Y, Liu Y, Tsai S-J, Lin C-P, et al. Structure-function coupling in white matter uncovers the abnormal brain connectivity in Schizophrenia. Transl Psychiatry. 2023;13:214.
27. Park B-Y, Hong S-J, Valk SL, Paquola C, Benkarim O, Bethlehem RAI, et al. Differences in subcortico-cortical interactions identified from connectome and microcircuit models in autism. Nat Commun. 2021;12:2225.
28. Di Martino A, O'Connor D, Chen B, Alaerts K, Anderson JS, Assaf M, et al. Enhancing studies of the connectome in autism using the autism brain imaging data exchange II. Sci Data. 2017;4:170010.
29. Lord C, Rutter M, DiLavore P, Risi S, Gotham K, Bishop S. Autism Diagnostic Observation Schedule. 2nd ed. West Psychol Corp. 2012.
30. Friston KJ, Williams S, Howard R, Frackowiak RS, Turner R. Movement-related effects in fMRI time-series. Magn Reson Med. 1996;35:346–55.
31. Peer M, Nitzan M, Bick AS, Levin N, Arzy S. Evidence for functional networks within the Human Brain's White Matter. J Neurosci. 2017;37:6394–407.
32. Gaser C, Dahnke R, Thompson PM, Kurth F, Luders E, Alzheimer's Disease Neuroimaging Initiative. CAT – A Computational Anatomy Toolbox for the Analysis of Structural MRI Data. Neuroscience; 2022. https://doi.org/10.1101/2022.06.11.495736
33. Mori S, Oishi K, Jiang H, Jiang L, Li X, Akhter K, et al. Stereotaxic white matter atlas based on diffusion tensor imaging in an ICBM template. NeuroImage. 2008;40:570–82.
34. Jones DK, Cercignani M. Twenty-five pitfalls in the analysis of diffusion MRI data. NMR Biomed. 2010;23:803–20.
35. Batchelor PG, Moakher M, Atkinson D, Calamante F, Connelly A. A rigorous framework for diffusion tensor calculus. Magn Reson Med. 2005;53:221–5.
36. Gao Y, Zhao Y, Li M, Lawless RD, Schilling KG, Xu L, et al. Functional alterations in bipartite network of white and grey matters during aging. NeuroImage. 2023;278:120277.
37. Bengio Y, Grandvalet Y. No unbiased estimator of the Variance of K-Fold Cross-validation. J Mach Learn Res. 2004;5:1089–105.
38. Kriegeskorte N, Simmons WK, Bellgowan PSF, Baker CI. Circular analysis in systems neuroscience: the dangers of double dipping. Nat Neurosci. 2009;12:535–40.
39. Vul E, Harris C, Winkielman P, Pashler H. Puzzlingly high correlations in fMRI studies of emotion, personality, and Social Cognition. Perspect Psychol Sci. 2009;4:274–90.

40. Rane RP, De Man EF, Kim J, Görgen K, Tschorn M, Rapp MA, et al. Structural differences in adolescent brains can predict alcohol misuse. eLife. 2022;11:e77545.
41. Ojala M, Garriga GC, Permutation Tests for Studying Classifier Performance, Ninth. IEEE Int Conf Data Min. Miami Beach, FL, USA: IEEE; 2009. pp. 908–13. http://ieeexplore.ieee.org/document/5360332/
42. Fortin J-P, Parker D, Tunç B, Watanabe T, Elliott MA, Ruparel K, et al. Harmonization of multi-site diffusion tensor imaging data. NeuroImage. 2017;161:149–70.
43. Chen X, Zhang H, Zhang L, Shen C, Lee S, Shen D. Extraction of dynamic functional connectivity from brain grey matter and white matter for MCI classification. Hum Brain Mapp. 2017;38:5019–34.
44. Zhuang W, Jia H, Liu Y, Cong J, Chen K, Yao D, et al. Identification and analysis of autism spectrum disorder via large-scale dynamic functional network connectivity. Autism Res. 2023;16:1512–26.
45. Arunachalam Chandran V, Pliatsikas C, Neufeld J, O'Connell G, Haffey A, DeLuca V, et al. Brain structural correlates of autistic traits across the diagnostic divide: a grey matter and white matter microstructure study. NeuroImage Clin. 2021;32:102897.
46. Chen K, Zhuang W, Zhang Y, Yin S, Liu Y, Chen Y, et al. Alteration of the large-scale white-matter functional networks in autism spectrum disorder. Cereb Cortex. 2023;33:11582–93.
47. Hong S-J, Hyung B, Paquola C, Bernhardt BC. The superficial White Matter in Autism and its role in Connectivity anomalies and Symptom Severity. Cereb Cortex. 2019;29:4415–25.
48. Yeh F-C, Irimia A, Bastos DCDA, Golby AJ. Tractography methods and findings in brain tumors and traumatic brain injury. NeuroImage. 2021;245:118651.
49. Aoki Y, Abe O, Nippashi Y, Yamasue H. Comparison of white matter integrity between autism spectrum disorder subjects and typically developing individuals: a meta-analysis of diffusion tensor imaging tractography studies. Mol Autism. 2013;4:25.
50. Wolff JJ, Gerig G, Lewis JD, Soda T, Styner MA, Vachet C, et al. Altered corpus callosum morphology associated with autism over the first 2 years of life. Brain. 2015;138:2046–58.
51. Wolff JJ, Swanson MR, Elison JT, Gerig G, Pruett JR, Styner MA, et al. Neural circuitry at age 6 months associated with later repetitive behavior and sensory responsiveness in autism. Mol Autism. 2017;8:8.
52. Frazier TW, Hardan AY. A Meta-analysis of the Corpus Callosum in Autism. Biol Psychiatry. 2009;66:935–41.
53. Hegarty JP, Monterrey JC, Tian Q, Cleveland SC, Gong X, Phillips JM, et al. A twin study of altered White Matter Heritability in Youth with Autism Spectrum Disorder. J Am Acad Child Adolesc Psychiatry. 2024;63:65–79.
54. Freitag CM, Luders E, Hulst HE, Narr KL, Thompson PM, Toga AW, et al. Total brain volume and Corpus Callosum Size in Medication-Naïve adolescents and young adults with Autism Spectrum Disorder. Biol Psychiatry. 2009;66:316–9.
55. Catani M, Jones DK, Daly E, Embiricos N, Deeley Q, Pugliese L, et al. Altered cerebellar feedback projections in Asperger syndrome. NeuroImage. 2008;41:1184–91.
56. Cheng Y, Chou K-H, Chen I-Y, Fan Y-T, Decety J, Lin C-P. Atypical development of white matter microstructure in adolescents with autism spectrum disorders. NeuroImage. 2010;50:873–82.
57. Shukla DK, Keehn B, Lincoln AJ, Müller R-A. White Matter Compromise of Callosal and Subcortical Fiber tracts in Children with Autism Spectrum disorder: a diffusion Tensor Imaging Study. J Am Acad Child Adolesc Psychiatry. 2010;49:1269–e12782.
58. Yeh F-C. Population-based tract-to-region connectome of the human brain and its hierarchical topology. Nat Commun. 2022;13:4933.
59. Hau J, Aljawad S, Baggett N, Fishman I, Carper RA, Müller R-A. The cingulum and cingulate U-fibers in children and adolescents with autism spectrum disorders. Hum Brain Mapp. 2019;40:3153.
60. Philippi CL, Mehta S, Grabowski T, Adolphs R, Rudrauf D. Damage to Association Fiber Tracts Impairs Recognition of the facial expression of emotion. J Neurosci. 2009;15089–99.
61. Shekari E, Nozari N. A narrative review of the anatomy and function of the white matter tracts in language production and comprehension. Front Hum Neurosci. 2023;17.
62. Yordanova YN, Duffau H, Herbet G. Neural pathways subserving face-based mentalizing. Brain Struct Funct. 2017;222:3087–105.
63. Andrews DS, Lee JK, Harvey DJ, Waizbard-Bartov E, Solomon M, Rogers SJ, et al. A longitudinal study of White Matter Development in relation to changes in Autism Severity Across Early Childhood. Biol Psychiatry. 2021;89:424–32.
64. Werring DJ, Brassat D, Droogan AG, Clark CA, Symms MR, Barker GJ, et al. The pathogenesis of lesions and normal-appearing white matter changes in multiple sclerosis: a serial diffusion MRI study. Brain. 2000;123:1667–76.
65. Ameis SH, Catani M. Altered white matter connectivity as a neural substrate for social impairment in Autism Spectrum Disorder. Cortex. 2015;62:158–81.
66. Baum GL, Cui Z, Roalf DR, Ciric R, Betzel RF, Larsen B, et al. Development of structure–function coupling in human brain networks during youth. Proc Natl Acad Sci. 2020;117:771–8.
67. Gu Z, Jamison KW, Sabuncu MR, Kuceyeski A. Heritability and interindividual variability of regional structure-function coupling. Nat Commun. 2021;12:4894.
68. Medaglia JD, Huang W, Karuza EA, Kelkar A, Thompson-Schill SL, Ribeiro A, et al. Functional alignment with Anatomical Networks is Associated with Cognitive Flexibility. Nat Hum Behav. 2018;2:156–64.
69. Vázquez-Rodríguez B, Suárez LE, Markello RD, Shafiei G, Paquola C, Hagmann P, et al. Gradients of structure–function tethering across neocortex. Proc Natl Acad Sci. 2019;116:21219–27.
70. Grisot G, Haber SN, Yendiki A. Diffusion MRI and anatomic tracing in the same brain reveal common failure modes of tractography. NeuroImage. 2021;239:118300.
71. Xie H, Chung DY, Kura S, Sugimoto K, Aykan SA, Wu Y, et al. Differential effects of anesthetics on resting state functional connectivity in the mouse. J Cereb Blood Flow Metab. 2020;40:875–84.
72. Xu S, Li M, Yang C, Fang X, Ye M, Wu Y, et al. Abnormal degree centrality in children with low-function Autism Spectrum disorders: a sleeping-state functional magnetic resonance imaging study. Neuropsychiatr Dis Treat. 2022;18:1363–74.
73. Zupin L, Sahyoun C, Krauss B, Dagri A, Rocco EM, Barbi E et al. Effectiveness of pharmacological procedural sedation in children with autism spectrum disorder: A systematic review and meta-analysis. Acta Paediatr. 2024;apa.17364.
74. Fong CY, Lim WK, Li L, Lai NM. Chloral hydrate as a sedating agent for neurodiagnostic procedures in children. Cochrane Epilepsy Group, editor. Cochrane Database Syst Rev. 2021;2021. https://doi.org/10.1002/14651858.CD011786.pub3

Publisher's note

Springer Nature remains neutral with regard to jurisdictional claims in published maps and institutional affiliations.